On the approximation of sound radiation by means of experiment-based optical full-field receptances

A. Zanarini
University of Bologna, Department of Industrial Engineering,
Viale Risorgimento 2, I-40136, Bologna, Italy
e-mail: **a.zanarini@unibo.it**

Abstract

This paper is focused on the exploitation of experiment-based optical full-field technologies in the sound radiation numerical simulation. Full-field *receptance* maps may cope with the challenges of the most advanced testing, useful to characterise, in the space and frequency domains, the specific structural dynamics of the actual set-up, with all the potential delays of the responses caught around the superposition of a modally dense dynamics, without the need of a FE model, especially in the case of lightweight structures or panels. The numerical approximation of the sound radiation field is here obtained by feeding the Rayleigh's integral formulation with the full-field experiment-based *receptances* obtained from a simple thin rectangular plate, designed as a lightweight structure to retain a complex structural dynamics, with its real constraints and damping characteristics. Examples are given on the modal superpositions and on the contribution of the experiment-based full-field *receptance* maps to the accuracy of the radiated acoustic pressure fields.

1 Introduction

Many times the sound radiation simulations from structural vibrations in the NVH environment are run with linear structural FE models, potentially simplified on the treatment of boundary conditions, frictions, mistuning from actual parts and nonlinearities. Moreover, the investigations may be found limited to a single tonal or resonance propagation, where just one effective eigenmode of the vibrating surface is used as distributed pressure source. Instead, working with operative deflection shapes, coming from broad frequency band real testing, may represent a viable path in order to have the best achievable representation of the real behaviour of manufactured and mounted components around their working load levels, also with modally dense structural dynamics and complex patterns in the dynamic signature of the excitations.

At their earlier steps, mostly qualitative and not competitive in terms of time-to-result [1], full-field measurements were mainly used to depict the response shape of a structure at a particular frequency of interest, due to the high spatial sampling offered and high consistency of each measurement degree of freedom with neighbouring locations [2]: a highly detailed spatial domain against the traditional coarse representation obtained by lumped sensor placement, with surface deflection shapes rapidly changing from frequency to frequency, functions of the complex superposition of the underneath eigensolutions in non-conventional patterns, giving relevant information on where to better locate the lumped vibration sensors or strain-gauges, the only quantitative instruments at that time.

Since the 1980s a non-native full field instrumentation like the SLDV has expanded the technique of contactless point measurement in time/frequency domains to a fine grid of locations, thus extending the concept of the velocity sensors to a spatially detailed acquisition, also adding no mass to the specimen. Thus SLDV was till recently considered *the reference* for the need of spatially detailed FRF measurements in NVH, because SLDV has kept the same peculiarities of previous technologies and proven procedures, just adding more dofs at a reasonable cost.

Native full field technologies, those based on an imaging sensor that acquires photons synchronously at every sensible site in an even denser grid, approach the measurement from another point of view, that of the ac-

knowledged quality obtainable in the spatial domain, especially in terms of consistency of the deflection field in the neighbouring dofs, as proved earlier by [3, 4]. Stroboscopic ESPI gives since the years 2000s [5, 6] an extremely accurate displacement field at the frequency of interest up to several kHz; but having data at all the lines of a broad frequency band can be prohibitive, due to time-consuming stepped sine excitation/acquisition, not automated till now. High-speed DIC, with its first commercial prototypes since around year 2005, has good detail in the time resolved displacement maps, though the extraction of the correlated fields is still very demanding in terms of calculation time. DIC can be more limited in the frequency domain, as the sensor/electronics bandwidth puts a trade-off between resolution and sampling rate, together with some limitations on the cameras' memory capacity, though under rapid electronics improvements.

The fundamental research project TEFFMA, funded by the European Commission and carried out by the author[1] at the Vienna University of Technology, aimed at making a comparison between the state-of-the-art in native full field technologies and the SLDV as reference, to understand at which point of their development these experimental procedures can provide NVH applications with enhanced peculiarities.

Although the works presented at ISMA2022 are a spin-off of the activities held during the TEFFMA project, they find their roots in the HPMI-CT-1999-00029 *Speckle Interferometry for Industrial Needs* Post-doctoral Marie Curie Industry Host Fellowship project at Dantec Ettemeyer GmbH. Since the testing in the latter (see [3, 4]) it became self-evident how ESPI measurements could give relevant mapping about the local behavior for enhanced structural dynamics assessments (see [6]) and fatigue spectral methods (see [7, 8]). The results in the former were the basis for the TEFFMA birth, whose works saw earlier presentations in 2014 [9,10], followed by consolidated reports in 2015 [11–14]. In [15] a gathering of the works of TEFFMA was firstly attempted, while in [16] an extensive description of the whole receptance estimation was faced and in [17] the EFFMA was detailed together with model updating attempts. The works in [18] underlined the quality of ESPI datasets in full-field dynamic testing. In [19] a precise comparison was made about new achievements for rotational and strain FRF high resolution maps. In [20] a risk index was first introduced as a metric to distinguish failure-exposed areas in a dynamically loaded component, with a focus also on the evidences from damaged fiberglass reinforced composite panels [21]. In the recent paper [22] the variability of risk maps was faced by the changes in the excitation dynamic signature, whereas [23] deals with the effects of different excitation locations. The attention on the high cycles fatigue life is clear as the sound pressure can be seen as distributed loading, therefore interwoven with NDT & risk grading procedures.

As described, many works [7–17, 19, 22] were already published by the author about the growing full-field optical technologies, their advantages and drawbacks in a broad frequency range. It was shown, especially in the latest works [9,12,15–17,19,22] from the TEFFMA project, how the growing native full-field techniques have started to offer tangible advances for the consistency and continuity of their data fields, with clear repercussions in model updating and derivative calculations (rotational dofs, strains, stresses, risk index maps). The reader can appreciate in [12, 15, 19] the effect of the measurement noise on the estimation of rotational dofs; though, unfortunately due to the complexity or burden of their measurement, the rotational dofs are usually disregarded, whilst they are relevant for the successful build of a reliable dynamic model for complex structures [24–29].

As the *experiment-based optical full-field testing* has proved [16,18] to be consistent in releasing high spatial resolution dynamic deflection shapes with reduced amount of noise on the fields, this paper is therefore focused on the exploitation of *experiment-based optical full-field technologies* in sound radiation numerical simulations. Therefore, they start to be a valid *non-contacting experiment-based* source of surface motion to explore in the approximation of the sound radiation, especially in the case of lightweight structures or panels. Optical technologies may cope with the challenges of the most demanding structural testing without the need of a FE model, like sensing the *full-field receptance maps* across a broad frequency range, useful to characterise, in the space and frequency domains, the specific structural dynamics of the actual set-up, with all the potential delays of the responses caught around the superposition of a modally dense dynamics.

The Rayleigh's integral formulation, recalled in Section 2, fed with the *full-field experiment-based receptances* obtained in the TEFFMA project, is here [30] investigated for the numerical approximation of the sound radiation field. The specimen under test was the simple thin rectangular plate of the TEFFMA project,

[1] A. Zanarini, scientific proposer & experienced researcher in the project TEFFMA - Towards Experimental Full Field Modal Analysis, financed by the Marie Curie FP7-PEOPLE-IEF-2011 PIEF-GA-2011-298543 grant, 1/02/2013 - 31/07/2015

designed as a lightweight structure to retain a complex structural dynamics within the operative ranges of the used measurement technologies, with its real constraints and damping characteristics. A recall of the experiment-based FRF modeling is sketched in Section 3, while a brief description of the testing is outlined in Section 4, with attentions on the set-up. In Section 5 examples are given in the space and frequency domains, after notes on the meshing of the acoustic domain, with special attention on the multi-modal superpositions, also outside the eigenfrequencies, and on the contribution of the *experiment-based full field receptance maps* to the accuracy of the radiated acoustic pressure FRFs and fields, before drawing the reader's attention to Section 6 for the final conclusions.

2 Sound pressure radiation formulation

In the case of propagating waves [31], according to [32–36], in the $a-th$ point of global coordinates $\boldsymbol{a}_a$ of the acoustic domain A, or air, the sound pressure $p(\boldsymbol{a}_a,\omega)$ can be defined from the Helmholtz's equation as:

$$p(\boldsymbol{a}_a,\omega)=\frac{i\omega\rho_0}{2\pi}\int_S v_n(\boldsymbol{q}_q,\omega)\frac{e^{-ikr_{aq}}}{r_{aq}}dS \tag{1}$$

or

$$p(\boldsymbol{a}_a,\omega)=2i\omega\rho_0\int_S v_n(\boldsymbol{q}_q,\omega)G(r_{aq},\omega)dS, G(r_{aq},\omega)=\frac{e^{-ikr_{aq}}}{4\pi r_{aq}}=\frac{e^{-i\omega r_{aq}/c_0}}{4\pi r_{aq}}, \tag{2}$$

where i is the imaginary unit, ω is the angular frequency ($\omega=2\pi h$, with h being the time frequency in Hertz), ρ_0 is the medium (air) density, $v_n(\boldsymbol{q}_q,\omega)$ is the normal (out-of-plane) velocity of the infinitesimal vibrating surface dS located in the global coordinate $\boldsymbol{q}_q$, $\boldsymbol{q}$ representing the whole vector of coordinates of the vibrating surface S, $k=\omega/c_0=2\pi/\lambda$ is the wavenumber in the Helmholtz's equation (c_0 is the speed of sound at rest in the medium, λ is the acoustic wavelength), $r_{aq}=\|\boldsymbol{r}_{aq}\|$ is the norm of the distance $\boldsymbol{r}_{aq}=\boldsymbol{a}_a-\boldsymbol{q}_q$ between the points in the two domains, and $G(r_{aq})$ is the free space Green's function as described in Eq.2.

Being the normal velocities in the frequency domain linked to the dynamic out-of-plane displacements over the static configuration $\boldsymbol{q}$, by means of the relation $\boldsymbol{v}_n(\boldsymbol{q},\omega)=-i\omega\boldsymbol{d}_n(\boldsymbol{q},\omega)$, which are expressions, by $\boldsymbol{d}_n(\boldsymbol{q},\omega)=\boldsymbol{H}_{\boldsymbol{d}_n\boldsymbol{q}f}(\omega)\cdot\boldsymbol{F}_f(\omega)$, of the *receptance FRFs* $\boldsymbol{H}_{\boldsymbol{d}_n\boldsymbol{q}f}(\omega)$ of size $N_q\times N_f$ - being N_q the number of the outputs and N_f of the inputs - and of the *excitation signatures* $\boldsymbol{F}_f(\omega)$, Eq.2 can be rewritten as below:

$$p(\boldsymbol{a}_a,\omega)=-2\omega^2\rho_0\int_S \boldsymbol{H}_{\boldsymbol{d}_{nqf}}(\omega)\boldsymbol{F}_f(\omega)G(r_{aq},\omega)dS\in\mathbb{C}, \tag{3}$$

with $\boldsymbol{H}_{\boldsymbol{d}_n\boldsymbol{q}f}(\omega)$, $\boldsymbol{F}_f(\omega)$ and $G(r_{aq},\omega)$ as *complex-valued* quantities, therefore also $p(\boldsymbol{a},\omega)\in\mathbb{C}$.

Note that normally $\boldsymbol{r}$ are considered as constant and *real-valued* vectors. It might be noted, instead, that $\boldsymbol{r}$ may become $\hat{\boldsymbol{r}}(\omega)=\boldsymbol{a}-\boldsymbol{q}-\boldsymbol{H}_{\boldsymbol{d}_n\boldsymbol{q}f}(\omega)\cdot\boldsymbol{F}_f(\omega)$, thus *complex-valued*. Nonetheless, being the contributions $\boldsymbol{H}_{\boldsymbol{d}_n\boldsymbol{q}f}(\omega)\cdot\boldsymbol{F}_f(\omega)$ of at least 3 orders of magnitude lower than the static distances $\boldsymbol{r}$ when far from the sound pressure source, at first evaluation they can be neglected, as well as the surface deflection that pushes the air in a direction slightly different from the actual normal, so that to consider $\boldsymbol{r}$ as constants at every frequency, with clear advantages in the amount and speed of calculations.

By means of a discretisation of the vibrating surface domain S that scatters the sound pressure, like $S\approx\sum_q\Delta S_q$, where ΔS_q is the discrete rectangular area of the surface with q-th point as centroid and dimensions as an average of the distances from the neighbor points in the grid, Eq.3 can be expressed in terms of a sum of discrete contributions:

$$p(\boldsymbol{a}_a,\omega)\approx-2\omega^2\rho_0\sum_q^{N_q}\boldsymbol{H}_{\boldsymbol{d}_nqf}(\omega)\boldsymbol{F}_f(\omega)G(r_{aq},\omega)\Delta S_q\in\mathbb{C}, \tag{4}$$

with $r_{aq}=\|\boldsymbol{r}_{aq}\|=\|\boldsymbol{a}_a-\boldsymbol{q}_q\|$.

Being $G(r_{aq}, \omega)$ and ΔS_q function of the locations of the N_a points in the acoustic domain and of the N_q points on the structure, they can be grouped in a *complex-valued* collocation matrix $\boldsymbol{T_{aq}}(\omega)$, sized $N_a \times N_q$, of element $\boldsymbol{T}_{aq}(\omega) = -2\rho_0 G(r_{aq}, \omega)\Delta S_q$, to transform Eq.4 into:

$$p(\boldsymbol{a}_a, \omega) \approx \omega^2 \boldsymbol{T_{aq}}(\omega)\boldsymbol{H_{d_n qf}}(\omega)\boldsymbol{F}_f(\omega) \in \mathbb{C}. \tag{5}$$

If, similarly to the *acoustic transfer vectors* in [37, 38], an *acoustic transfer matrix* $\boldsymbol{V_{aq}}(\omega)$ is defined as $\boldsymbol{V_{aq}}(\omega) = \omega^2 \cdot \boldsymbol{T_{aq}}(\omega) \cdot \boldsymbol{H_{d_n qf}}(\omega) \in \mathbb{C}$, product of the rectangular collocation matrix $\boldsymbol{T_{aq}}(\omega)$ times the *receptance* matrix $\boldsymbol{H_{d_n qf}}(\omega)$ and ω^2, Eq.5 can be easily rewritten as:

$$p(\boldsymbol{a}_a, \omega) \approx \boldsymbol{V_{aq}}(\omega)\boldsymbol{F}_f(\omega) \in \mathbb{C}, \tag{6}$$

useful in the cases where the structural response and acoustic domains are kept while varying the excitation signature to map the responses on the acoustic pressure.

Therefore, once the acoustic domain geometry has been defined, the geometry of the radiating surface - of the output points where the *receptance FRFs* $\boldsymbol{H_{d_n qf}}(\omega)$ was estimated - easily leads to the evaluation of the collocation matrix $\boldsymbol{T_{aq}}(\omega)$, and allows the estimation of the pressure field by means of matrix multiplications.

Note also that Eq.5 permits the calculation of the sound pressure field directly from *experiment-based full-field receptances*, which should help the accuracy of the results, thanks to the high spatial resolution and because these *receptances* retain the blending of any complex-valued ODS active at the specific frequency, with the proper real boundaries and dissipation effects of the vibrating structure.

3 Full Field FRFs: direct experimental modelling

All the activities in the TEFFMA project gravitate around impedance based studies by means of full field optical measurements, in order to obtain highly reliable Full Field FRFs with unprecedented spatial resolutions, for any further speculation that may come either from experimental test or from numerical models, also in hybrid frameworks.

3.1 Brief recall of a direct characterisation

The well known formulation [24,27] of *receptance* matrix $\boldsymbol{H_d}(\omega)$, as spectral relation between displacements and forces, will be used for the Full Field FRF estimation, describing the dynamic behaviour of a testing system, with potentially multi-input excitation, here 2 distinct shakers, and *many*-output responses, here also several thousands, covering the whole sensed surface, as can be formulated in the following complex-valued equation:

$$H_{d_{qf}}(\omega) = \frac{\sum_{k=1}^{N} S^k_{X_q F_f}(\omega)}{\sum_{k=1}^{N} S^k_{F_f F_f}(\omega)} \in \mathbb{C} \tag{7}$$

where X_q is the output displacement at q-th dof induced by the input force F_f at f-th dof, while $S^k_{X_q F_f}(\omega)$ is the k-th cross power spectral density between input and output, $S^k_{F_f F_f}(\omega)$ is the k-th auto power spectral density of the input and ω is the frequency, evaluated in N repetitions.

Once the specific excitation signature $F_f(\omega)$ is known in the frequency domain, the FRF formulation in Eq.7 can be used to obtain the full field displacements over the entire surface, as follows at specific output dof q:

$$d_{qf}(\omega) = H_{d_{qf}}(\omega)F_f(\omega) \in \mathbb{C} \tag{8}$$

or for the whole displacement vector $\boldsymbol{d}_f$ due to excitation in a single dof f as:

$$\boldsymbol{d}_f(\omega) = \boldsymbol{H_{df}}(\omega)F_f(\omega) \in \mathbb{C} \tag{9}$$

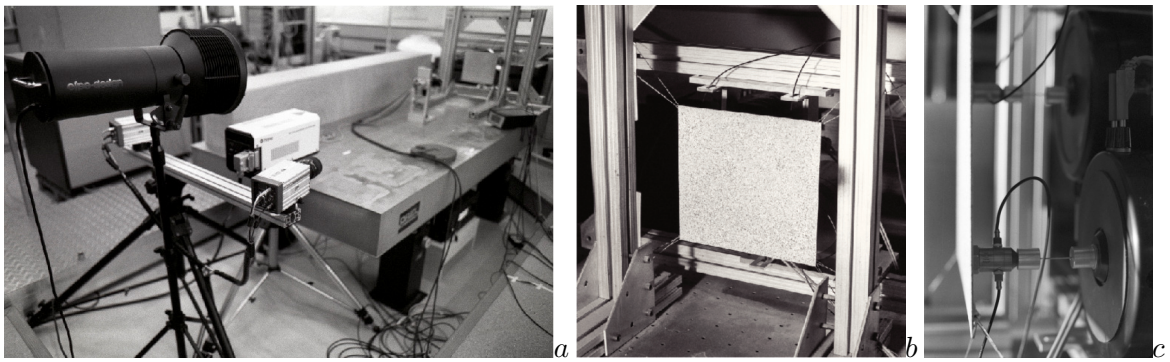

Figure 1: Full field measurement instruments gathered in front of the specimen at the optical anti-vibration table with backside shakers: the instruments in a, the restrained thin plate in b and the 2 shakers in c.

Increasing the spatial resolution in dynamic models by means of *many* dofs Full Field FRFs will be therefore a valuable addition to the state-of-the-art of the design of complex systems and will surely lead to the exploration of new FRF-based quantities derived from enhanced quality displacement fields, such as surface rotations, strains & stresses and failure point distributions [12–15, 17, 19]. Furthermore, distributed loading patterns, such as those coming from vibro-acoustics [30], might be considered.

4 Activities in the lab of TU-Wien for the TEFFMA project

The well equipped laboratory of the TU-Wien made possible a complex set-up for the comparison of the qualities of three different technologies available in acquiring Full Field FRFs (as best detailed in [16]): SLDV, Hi-Speed DIC and Dynamic ESPI.

4.1 Summary of the technological equipment

During the time of the measurements the laboratory facility at TU-Wien had an underground dedicated room with seismic floor and air-cushion anti-vibration optical table, to filter out the environmental vibrations. A Polytec PSV 300 was at disposal, with 1D (out-of-plane) scanning head OFV-056. Due to its peculiarities of being the junction instrument between the traditional NVH measurement technologies and the growing native full field equipment, SLDV was taken as reference. Besides, it must be recalled that SLDV delivers velocities and not displacements. The native full field equipment consisted in the Dantec Ettemeyer Q-500 Hi-Res, the ESPI system for 3D dynamic measurements in stroboscopic coherent laser light, and in the Dantecdynamics Q-450, for 3D dynamic DIC acquisitions by means of hi-speed cameras (Nanosense Mk III) in high frequency & power white light.

It was clear since the beginning that there were differences in both spatial and frequency domains (more details in [16]). For the physics of each instrumentation see instead [1, 2, 39–41]. In particular, ESPI was plenty of spatial resolution (even 1 million dofs) with very clean datasets [16, 17, 19], but required stepped sine excitation, up to many kHz, resulting in a long and cumbersome data acquisition, especially if all the needed frequency lines were tightly spaced, as in the TEFFMA project. Great attention was paid to understand the limits & requirements of all these technologies in order to find a common intersection of measurements conditions: there resulted a promising compromise in the range [20 - 1024] Hz, with the 3 techniques having their own spatial and frequency resolutions. The linearity was checked by some comparative tests with varying input power, to be able to compare measurements done at three different source power levels.

4.2 Brief experimental set-up description

The experimental set-up was designed in order to let all the three measurement technologies focus on the same dynamic behavior, as this was decided to be populated by a high modal density inside the frequency

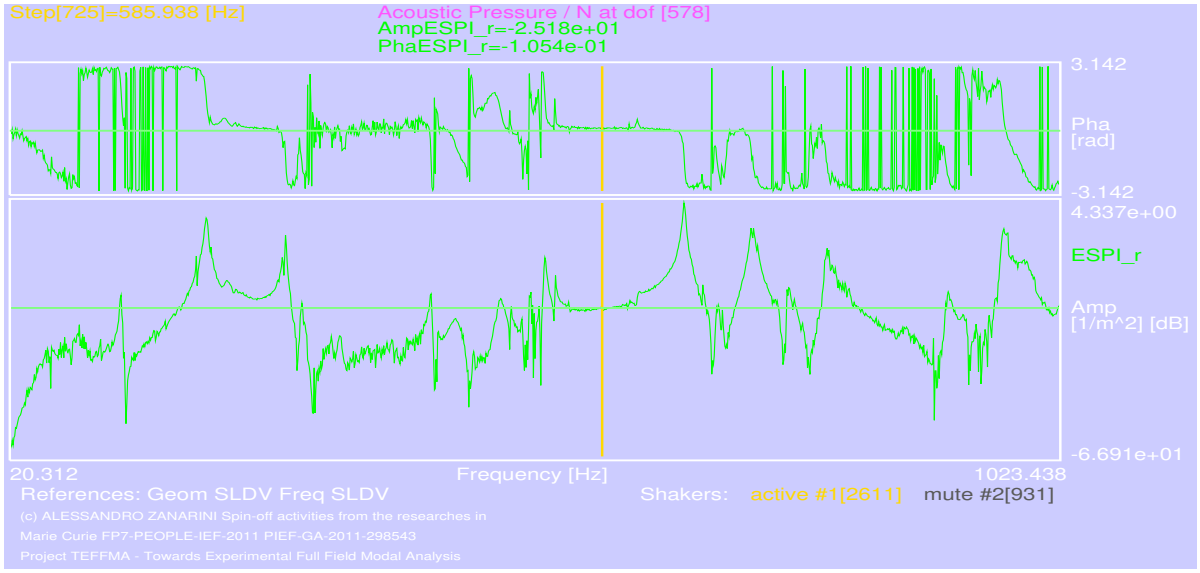

Figure 2: Example of *acoustic transfer matrix* graph in the frequency domain evaluated in acoustic dof 578 from shaker 1.

range of interest. An aluminum rectangular thin plate (dimensions: 250 x 236 x 1.5 mm) was tightened by wires fixed to a solid frame on the air-spring optical table (see Fig.1) to restrain excessive rigid body movement. The surface of the plate was sprayed with a random noise pattern paint layer to full-fill the requirements of DIC. The excitation was given by electrodynamic shakers positioned on the back side of the plate, to full-fill the stepped-sine acquisition procedure for dynamic ESPI measurements and the requirements for SLDV and DIC. LMS Test.Lab drove the excitation in SLDV and DIC measurements, while ESPI system used an external sine waveform generator, synchronised with the phase-shifting procedures. To be able to calculate the *receptance* FRFs as in Eq.7, force signal was sampled at the shaker-plate interfaces by means of the force cells in the impedance heads.

4.3 Pre-testing the rig for optimal results

As already explained in [16], the tuning of the set-up went far beyond the traditional selection of the best acquisition parameters for each technology, being ESPI in the bunch of the techniques. ESPI permitted unprecedented fine tuning of the rig, by means of a precise adjustment of the nuts on the restraints, when the dynamic analysis was carried out at much higher frequencies than those in the common overlapping. ESPI strongly helped in assessing, fixing and thus preventing unwanted vibrations from any part of the rig up to 6500 Hz, just above the Nyquist frequency for SLDV: this means that the output motion of the plate was highly coherent with the input force [9, 15, 16], for the best achievable measurements.

Great attention was also paid to the optical alignments of all the instruments, in all the directions/rotations; also the depth of field of each optics was accurately selected to match the structural dynamics requirements, in terms of collected photons and dynamic range for the best image quality.

The gained experience with full-field optical measurements revealed itself, together with the extended practice of photography of the author[2], as pivotal in arranging the multiple camera acquisition for photogrammetry [41] tests in [42, 43].

4.4 Estimating full-field FRFs from optical measurements

Once the methodology above is defined, *receptance FRF maps* at specific frequencies and excitation sources can be obtained as in Section 3. The datasets here retained are based on the geometry grid of SLDV inside the

[2]Fine art, nature and wildlife photography at `https://www.colorazeta.it/index_EN.htm`

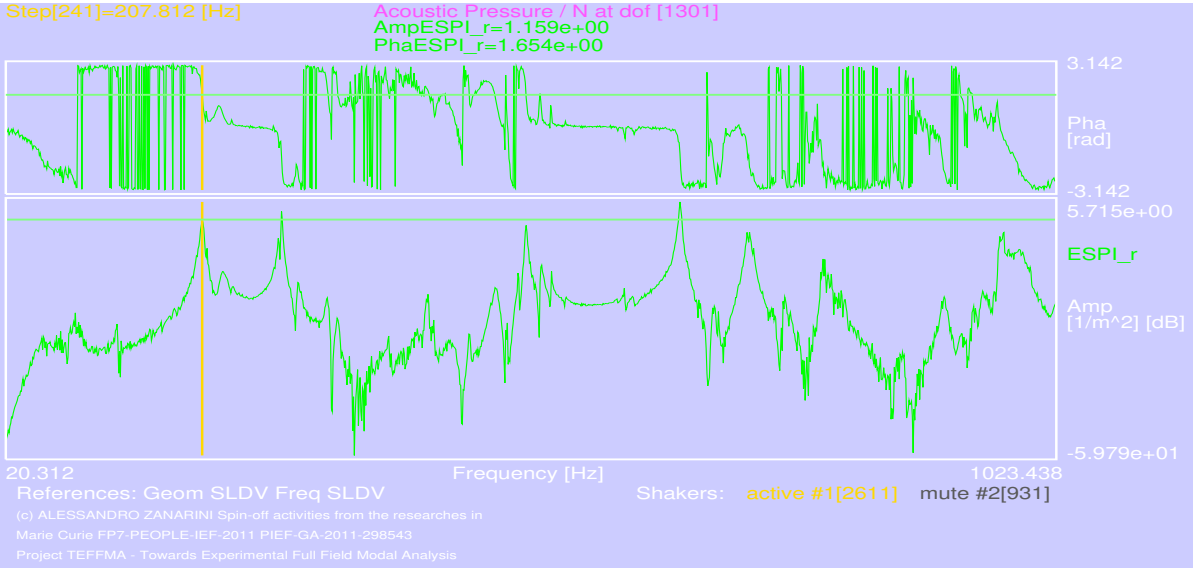

Figure 3: Example of *acoustic transfer matrix* graph in the frequency domain evaluated in acoustic dof 1301 from shaker 1.

plate area (57 x 51 dofs, less than 4 mm among each dof, in Eq.5 $N_q = 2907$), and on the [20.312–1023.438] Hz frequency range, with a spectral even spacing of 0.78125 Hz among the 1285 frequency lines. The interested reader can widen the understanding in [15, 16], to appreciate the spatial consistency & continuity of the data, with clean shapes, sharp nodal lines and excellent *Coherence*, especially from ESPI. The latter was here used as the most clean source available of experimental data for the specific purpose of simulating the sound radiation pressure of Eq.6, as follows.

5 Sound pressure mapping from full-field *receptances*

As highlighted in Section 2, the motion of the sound radiating surface can be modelled by means of the *experiment-based receptances* obtained from Sections 3 & 4. In particular, from Eq.6, it is clear how relevant is the evaluation of the defined *acoustic transfer matrix* $\boldsymbol{V_{aq}}(\omega)$, before the adoption of a specific excitation signature, to simulate the acoustic pressure in the acoustic domain.

5.1 Meshing the acoustic domain

For the proofs of the introduced concepts, a simple 3D space meshing routine was prepared, with different grid geometries available, upon which to discretise the locations of the virtual pressure receivers. The main options are: i) a flat rectangular grid; ii) part of a cylindrical grid; iii) part of a spherical grid. Each grid can be oriented and positioned in the 3D space, relative to the vibrating surface.

The number of nodes in the grid has no specific limit, but the underneath parallel computing strategy tested can take advantage of up to 51x51 nodes in the grid[3], thanks to the common positioning vectors $\boldsymbol{r_{aq}}$ in the Green's functions and in Eqs.4-6 between structural and acoustic domains, which may be evaluated just once and kept afterwards in memory for each frequency line, in the displacement field approximation adopted.

For the aims of this paper, a rectangular mesh was generated, of size $0.5m \times 0.5m$, with 51×51 dofs ($N_a = 2601$, $10mm$ among each dof), centered on the vibrating plate and positioned $0.1m$ above it. The medium (air) parameters were fixed in $c_0 = 300.0m/s$ and $\rho_0 = 1.204kg/m^3$.

[3]Limit fixed to use 145GB of RAM, based on C language OpenMP code, in Linux environment, and on 192 GB of RAM and 12 physical cores in a workstation with dual hexacore Intel® Xeon® X5690 running at 3.46 GHz.

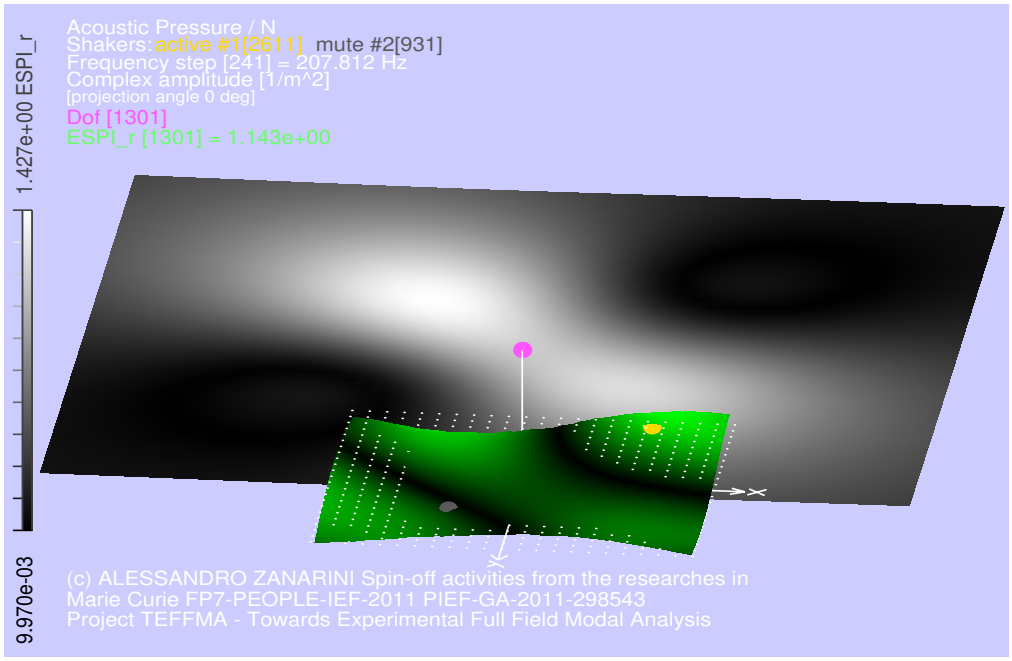

Figure 4: Example of *acoustic transfer matrix* mesh evaluated at the specific frequency of 208 Hz from shaker 1.

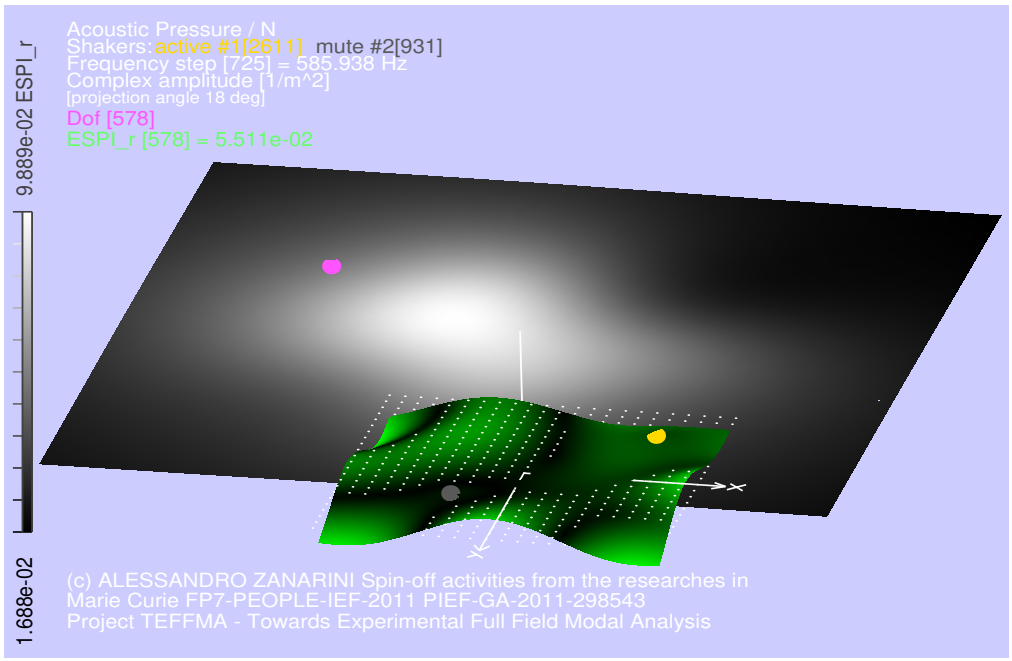

Figure 5: Example of *acoustic transfer matrix* mesh evaluated at the specific frequency of 586 Hz from shaker 1.

5.2 Evaluation of the *acoustic transfer matrix*

The core of this paper is to show the possibility to evaluate the *acoustic transfer matrix* $\boldsymbol{V_{aq}}(\omega)$ directly from the *experiment-based receptances*, as proposed in Section 2, without the need of any FE structural model, but with great detail and field quality. As Sections 3 & 4 highlighted, accurate *receptance* matrices $\boldsymbol{H_{d_n qf}}(\omega)$ can be estimated with high resolution in spatial and frequency domains from both shakers available in the TEFFMA project. In Fig.2 an example is reported as a frequency domain relation from shaker 1 and acoustic

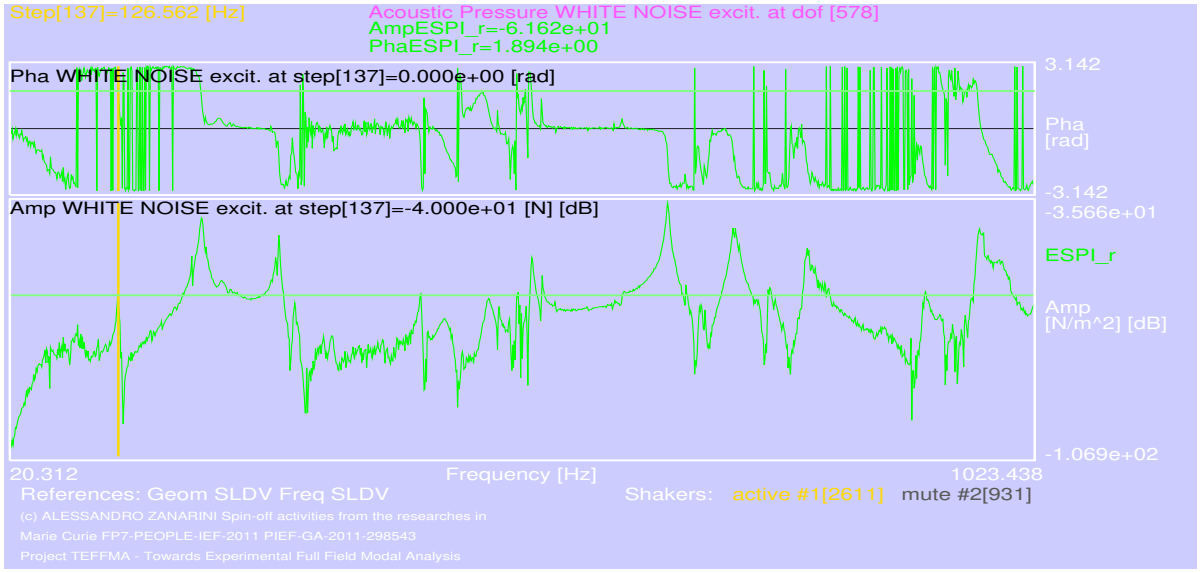

Figure 6: Example of *acoustic pressure* graph in the frequency domain evaluated in acoustic dof 578 with *white noise* excitation from shaker 1.

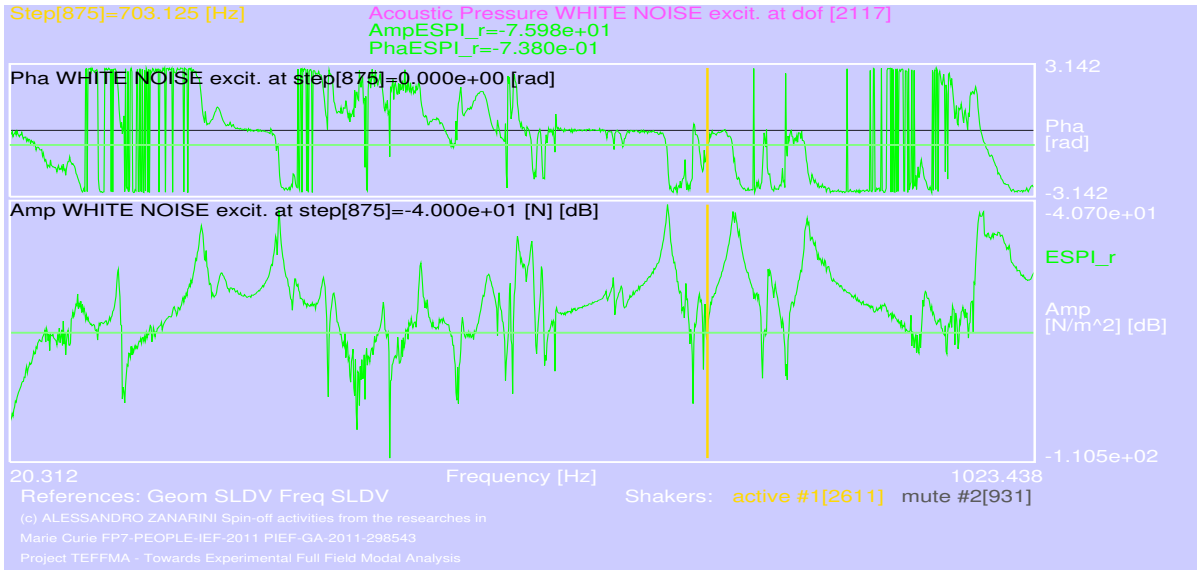

Figure 7: Example of *acoustic pressure* graph in the frequency domain evaluated in acoustic dof 2117 with *white noise* excitation from shaker 1.

dof 578 here selected in the rectangular acoustic mesh. Another example of acoustic transfer matrix single dof graph appears in Fig.3 at dof 1301, to highlight the variability of the acoustic pressure FRF among the dofs of the acoustic mesh. It is important to underline how the *acoustic transfer matrix* obtained from the *experiment-based receptances* preserves, with its *complex-valued nature*, the real life conditions of the test, without any simplification in the damping, nor in the modal base truncation or identification.

Instead, in Fig.4, the *acoustic transfer matrix* results of acoustic pressure over force are shown over the entire acoustic mesh, retaining again the *complex-valued* relations and phase delays, coming from the underneath *complex-valued receptance* matrix $\boldsymbol{H}_{\boldsymbol{d}_n\boldsymbol{q}\boldsymbol{f}}(\omega)$, but blended in the *complex-valued* summation in $\boldsymbol{V}_{\boldsymbol{a}\boldsymbol{q}}(\omega)$. To be noted that the *acoustic FRF maps* (acoustic pressure over force) are displayed in grey tones, whereas the corresponding *receptance maps* (displacement over force), here adjoined to give a clear link to the radiating shape, have the green tones, used in the TEFFMA project to display ESPI-based structural datasets. Brighter tones are used for range maximum, dark tones for minimum, in both acoustic and structural domains, with a

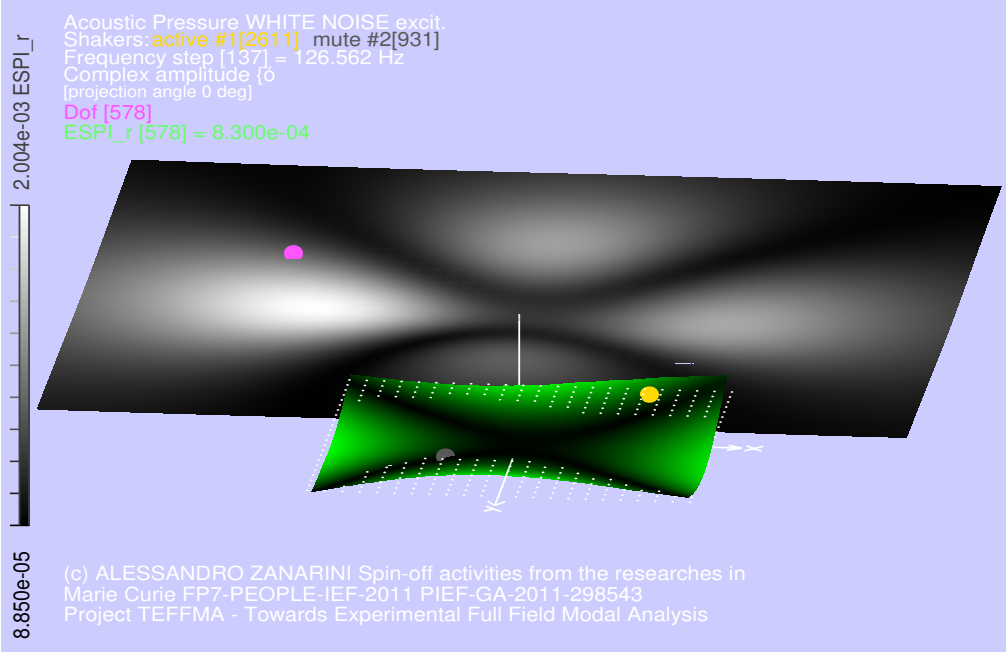

Figure 8: Example of *acoustic pressure* mesh evaluated at the specific frequency of 127 Hz from shaker 1.

linear tone grading based on the amplitude specifically depicted (real part, imaginary part, complex amplitude and phase). An axes triad and a net of dots, at zero Z-elevation from the plate, complete the tools to visualise these complex-valued fields. In Fig.5 the *acoustic transfer matrix* is depicted at a higher frequency, when the acoustic pressure has a more complex pattern. It appears also manifest how the distance on the acoustic mesh, as expected, plays a relevant role in blending, or averaging, the contributions of specific areas on the vibrating plate, revealing in particular the proximity to specific nodal lines of the structural ODSs.

5.3 Evaluation of the acoustic pressure field with coloured noise excitation

The amplitude spectrum of the coloured noise $F_{C_\alpha}(\omega)$, here used as the force excitation, can be simply modelled as a real valued function in the ω frequency, yielding:

$$F_{C_\alpha}(\omega) = \frac{F_0}{(\omega)^\alpha} \tag{10}$$

with $\alpha \in [-2, 2]$ defining the noise color ($\alpha = -2$ for *violet noise*, $\alpha = -1$ for *blue noise*, $\alpha = 0$ for *white noise*, $\alpha = 1$ for *pink noise* and $\alpha = 2$ for *red noise*) and with F_0 intended as the reference amplitude of the excitation force in the frequency range. No assumptions on the relative phase among the components on the frequency axis were made, thus the phases were kept fixed to null delay for all the lines by means of real numbers. The use of *complex-valued* input spectra changes only the product in Eq.6, being all the quantities then complex-valued. Therefore a *red noise* highly exalts the lower frequency region of the *acoustic pressure FRFs*, a *white noise* gives the same energy to all the frequency lines and a *violet noise* gives a strong power to the higher frequency structural dynamics, with the *pink noise* and *blue noise* as intermediate situations, aside of the neutral *white noise*, here adopted for an equal energy balance in all the frequency lines.

In the proof here organised, the *white noise* amplitude spectrum was used with $F_0 = 0.01$ N, with excitation from shaker 1. As can be seen in Fig.6, the complex-valued acoustic pressure in dof 578 is depicted as it was its acoustic transfer matrix function of Fig.2, with just the scaling change due to the adopted F_0 in the the *white noise* excitation. Instead, a different excitation complex spectrum would have influenced the scaling in complex amplitude and phase of each spectral contribution. In Fig.7 the acoustic pressure is depicted in another dof (2117) of the acoustic mesh, to show its variability coming from the simulated location of the receiver.

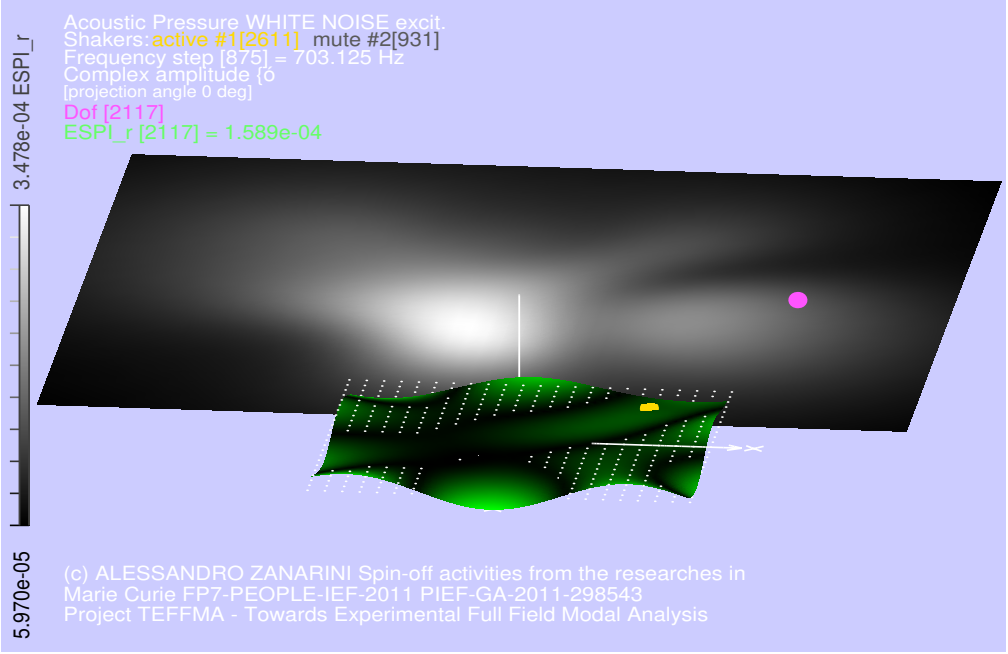

Figure 9: Example of *acoustic pressure* mesh evaluated at the specific frequency of 703 Hz from shaker 1.

In Fig.8 the acoustic pressure field is shown to exhibit a clear link to the underneath *receptance* shape, as the latter is quite simple at 127 Hz. As the frequency rises, more complexity pertains the *receptance* maps, as can be clearly seen in Fig.9 at 703 Hz, but the resulting complex-valued blending in the acoustic pressure field, taking account of all the contributions across the radiating surface, properly phased, now has a different shape, coming from the complex-valued summation of 2907 contributing Green's functions in Eq.2.

6 Conclusions

This paper has highlighted the possibilities in NVH coming from *experiment-based full-field tools*, specifically the optical full-field measurements, for an advancement of experimental benchmarks of design procedures of complex structures. The unprecedented mapping ability, in both spatial and frequency domain, coming from the *experiment-based full-field receptances*, opens new vibro-acoustic prediction scenarios, as the real-life structural dynamics of the radiating surface is entirely retained in the FRFs with great accuracy, but without assumptions in the damping nor errors in any modal identification nor FE model updating.

Nonetheless, experiments to benchmark the sound radiation predictions have in future to further give assurance of the achieved results, for an increased awareness of the qualities of the full-field measurements in dynamic testing of structures for the most demanding vibro-acoustic radiation predictions.

The path towards experimental Full-Field NVH is paved with promising advancements.

Acknowledgements

This activity is a spin-off of the Project TEFFMA - Towards Experimental Full Field Modal Analysis, funded by the European Commission at the Technische Universitaet Wien, through the Marie Curie FP7-PEOPLE-IEF-2011 PIEF-GA-2011-298543 grant, for which the Research Executive Agency is greatly acknowledged. TU-Wien, in the person of Prof. Wassermann and his staff, are kindly acknowledged for having hosted the TEFFMA project of the author at the *Schwingungs- und Strukturanalyse* / Optical Vibration Measurement Laboratory. The workstation used to extensively process the datasets and code the acoustic radiation was provided by the author on his own savings.

References

[1] P. K. Rastogi, *Optical Measurement Techniques and Applications*. Nordwood, MA 02062, U.S.A.: Artech House, Inc., 1997.

[2] T. Kreis, *Handbook of Holographic Interferometry*. Berlin, Germany: Wiley-VCH, 2004.

[3] A. Zanarini, "Dynamic behaviour carachterization of a brake disc by means of electronic speckle pattern interferometry measurements," in *Proceedings of the IDETC/CIE ASME International Design Engineering Technical Conferences & Computers and Information in Engineering Conference, Long Beach, California, USA, September 24-28*. ASME, 2005, pp. 273–280, paper DETC2005-84630. [Online]. Available: https://doi.org/10.1115/DETC2005-84630

[4] A. Zanarini, "Damage location assessment in a composite panel by means of electronic speckle pattern interferometry measurements," in *Proceedings of the IDETC/CIE ASME International Design Engineering Technical Conferences & Computers and Information in Engineering Conference, Long Beach, California, USA, September 24-28*. ASME, 2005, pp. 1–8, paper DETC2005-84631. [Online]. Available: https://doi.org/10.1115/DETC2005-84631

[5] H. Van der Auweraer, H. Steinbichler, C. Haberstok, R. Freymann, D. Storer, and V. Linet, "Industrial applications of pulsed-laser espi vibration analysis," in *Proc. of the XIX IMAC, Kissimmee, FL, USA*. SEM, 2001, pp. 490–496. [Online]. Available: https://www.researchgate.net/publication/238246330_Industrial_Applications_of_Pulsed-Laser_ESPI_Vibration_Analysis

[6] A. Zanarini, "Full field ESPI measurements on a plate: challenging experimental modal analysis," in *Proceedings of the XXV IMAC, Orlando (FL) USA, Feb 19-22*. SEM, 2007, pp. 1–11, paper s34p04. [Online]. Available: https://www.researchgate.net/publication/266896551_Full_field_ESPI_measurements_on_a_plate_Challenging_Experimental_Modal_Analysis

[7] A. Zanarini, "Fatigue life assessment by means of full field ESPI vibration measurements," in *Proceedings of the ISMA2008 Conference, September 15-17, Leuven (Belgium)*, P. Sas, Ed. KUL, 2008, pp. 817–832, Condition monitoring, Paper 326. [Online]. Available: https://doi.org/10.13140/RG.2.1.3452.9365

[8] A. Zanarini, "Full field ESPI vibration measurements to predict fatigue behaviour," in *Proceedings of the IMECE2008 ASME International Mechanical Engineering Congress and Exposition, October 31- November 6, Boston (MA) USA*. ASME, October 31- November 6 2008, pp. 165–174, paper IMECE2008-68727. [Online]. Available: https://doi.org/10.1115/IMECE2008-68727

[9] A. Zanarini, "On the estimation of frequency response functions, dynamic rotational degrees of freedom and strain maps from different full field optical techniques," in *Proceedings of the ISMA2014 including USD2014 - International Conference on Noise and Vibration Engineering, Leuven, Belgium, September 15-17*. KU Leuven, September 15-17 2014, pp. 1177–1192, Dynamic testing: methods and instrumentation, paper ID676. [Online]. Available: http://past.isma-isaac.be/downloads/isma2014/papers/isma2014_0676.pdf

[10] A. Zanarini, "On the role of spatial resolution in advanced vibration measurements for operational modal analysis and model updating," in *Proceedings of the ISMA2014 including USD2014 - International Conference on Noise and Vibration Engineering, Leuven, Belgium, September 15-17*. KU Leuven, September 15-17 2014, pp. 3397–3410, Operational modal analysis, paper ID678. [Online]. Available: http://past.isma-isaac.be/downloads/isma2014/papers/isma2014_0678.pdf

[11] A. Zanarini, "Comparative studies on full field FRFs estimation from competing optical instruments," in *Proceedings of the ICoEV2015 International Conference on Engineering Vibration, Ljubljana, Slovenia, September 7-10*. Univ. Ljubljana & IFToMM, September 7-10 2015, pp. 1559–1568, ID191. [Online]. Available: https://www.researchgate.net/publication/280013709_Comparative_studies_on_Full_Field_FRFs_estimation_from_competing_optical_instruments

[12] A. Zanarini, "Accurate FRFs estimation of derivative quantities from different full field measuring technologies," in *Proceedings of the ICoEV2015 International Conference on Engineering Vibration, Ljubljana, Slovenia, September 7-10*. Univ. Ljubljana & IFToMM, September 7-10 2015, pp. 1569–1578, ID192. [Online]. Available: https://www.researchgate.net/publication/280013778_Accurate_FRF_estimation_of_derivative_quantities_from_different_full_field_measuring_technologies

[13] A. Zanarini, "Full field experimental modelling in spectral approaches to fatigue predictions," in *Proceedings of the ICoEV2015 International Conference on Engineering Vibration, Ljubljana, Slovenia, September 7-10*. Univ. Ljubljana & IFToMM, September 7-10 2015, pp. 1579–1588, ID193. [Online]. Available: https://www.researchgate.net/publication/280013788_Full_field_experimental_modelling_in_spectral_approaches_to_fatigue_predictions

[14] A. Zanarini, "Model updating from full field optical experimental datasets," in *Proceedings of the ICoEV2015 International Conference on Engineering Vibration, Ljubljana, Slovenia, September 7-10*. Univ. Ljubljana & IFToMM, September 7-10 2015, pp. 773–782, ID196. [Online]. Available: https://www.researchgate.net/publication/280013876_Model_updating_from_full_field_optical_experimental_datasets

[15] A. Zanarini, "Broad frequency band full field measurements for advanced applications: Point-wise comparisons between optical technologies," *Mechanical Systems and Signal Processing*, vol. 98, pp. 968 – 999, 2018. [Online]. Available: https://doi.org/10.1016/j.ymssp.2017.05.035

[16] A. Zanarini, "Competing optical instruments for the estimation of Full Field FRFs," *Measurement*, vol. 140, pp. 100 – 119, 2019. [Online]. Available: https://doi.org/10.1016/j.measurement.2018.12.017

[17] A. Zanarini, "Full field optical measurements in experimental modal analysis and model updating," *Journal of Sound and Vibration*, vol. 442, pp. 817 – 842, 2019. [Online]. Available: https://doi.org/10.1016/j.jsv.2018.09.048

[18] A. Zanarini, "On the making of precise comparisons with optical full field technologies in NVH," in *Proceedings of the ISMA2020 including USD2020 - International Conference on Noise and Vibration Engineering, Leuven, Belgium, September 7-9*. KU Leuven, September 7-9 2020, pp. 2293–2308, Optical methods and computer vision for vibration engineering, paper ID 695. [Online]. Available: https://www.researchgate.net/publication/344353185_On_the_making_of_precise_comparisons_with_optical_full_field_technologies_in_NVH

[19] A. Zanarini, "Chasing the high-resolution mapping of rotational and strain FRFs as receptance processing from different full-field optical measuring technologies," *Mechanical Systems and Signal Processing*, vol. 166, p. 108428, 2022. [Online]. Available: https://doi.org/10.1016/j.ymssp.2021.108428

[20] A. Zanarini, "On the defect tolerance by fatigue spectral methods based on full-field dynamic testing," *Procedia Structural Integrity*, vol. 37, pp. 525–532, 2022, paper ID 105, ICSI 2021 The 4th International Conference on Structural Integrity. [Online]. Available: https://doi.org/10.1016/j.prostr.2022.01.118

[21] A. Zanarini, "On the exploitation of multiple 3D full-field pulsed ESPI measurements in damage location assessment," *Procedia Structural Integrity*, vol. 37, pp. 517–524, 2022, paper ID 104, ICSI 2021 The 4th International Conference on Structural Integrity. [Online]. Available: https://doi.org/10.1016/j.prostr.2022.01.117

[22] A. Zanarini, "Introducing the concept of defect tolerance by fatigue spectral methods based on full-field frequency response function testing and dynamic excitation signature," *International Journal of Fatigue*, vol. 165, p. 107184, 2022. [Online]. Available: https://doi.org/10.1016/j.ijfatigue.2022.107184

[23] A. Zanarini, "About the excitation dependency of risk tolerance mapping in dynamically loaded structures," in *Proceedings of the ISMA2022 including USD2022 - International Conference on Noise and*

Vibration Engineering, Leuven, Belgium, September 12-14. KU Leuven, September 12-14 2022, pp. 1–15, paper ID 208.

[24] W. Heylen, S. Lammens, and P. Sas, *Modal Analysis Theory and Testing*, 2nd ed. Leuven (Belgium): Katholieke Universiteit Leuven, 1998, ISBN 90-73802-61-X.

[25] W. Liu and D. Ewins, "The Importance Assessment of RDOF in FRF Coupling Analysis," in *Proceedings of the IMAC 17th Conference, Kissimmee, Florida*, 1999, pp. 1481–1487, Society for Experimental Mechanics (SEM). [Online]. Available: http://www3.imperial.ac.uk/pls/portallive/docs/1/49146.PDF

[26] Research network, "QUATTRO Brite-Euram project no: BE 97-4184," European Commision Research Framework Programs, Tech. Rep., 1998.

[27] D. J. Ewins, *Modal Testing - theory, practice and application*, 2nd ed. Baldock, Hertfordshire, England: Research Studies Press Ltd., 2000. [Online]. Available: https://www.wiley.com/en-it/Modal+Testing%3A+Theory%2C+Practice+and+Application%2C+2nd+Edition-p-9780863802188

[28] M. Friswell and J. E. Mottershead, *Finite Element Model Updating in Structural Dynamics*, ser. Solid Mechanics and Its Applications. Kuwler Academic Publishers, Springer Netherlands, 1995.

[29] M. Haeussler, S. Klaassen, and D. Rixen, "Experimental twelve degree of freedom rubber isolator models for use in substructuring assemblies," *Journal of Sound and Vibration*, vol. 474, p. 115253, 2020. [Online]. Available: http://www.sciencedirect.com/science/article/pii/S0022460X20300845

[30] A. Zanarini, "On the approximation of sound radiation by means of experiment-based optical full-field receptances," in *Proceedings of the ISMA2022 including USD2022 - International Conference on Noise and Vibration Engineering, Leuven, Belgium, September 12-14*. KU Leuven, September 12-14 2022, pp. 1–15, paper ID 207.

[31] P. Mas and P. Sas, "Acoustic source identification based on microphone array processing," Katholieke Universiteit Leuven, Belgium, Mechanical Engineering Department, Noise & Vibration research group, Tech. Rep., 2004, In ISAAC 15 - Course on numerical and applied acoustics, Katholieke Universiteit Leuven, Belgium, Mechanical Engineering Department, Noise & Vibration research group, URL: https://www.isma-isaac.be.

[32] S. Kirkup, "Computational solution of the acoustic field surrounding a baffled panel by the rayleigh integral method," *Applied Mathematical Modelling*, vol. 18, no. 7, pp. 403–407, 1994. [Online]. Available: https://www.sciencedirect.com/science/article/pii/0307904X94902275

[33] W. Desmet, "Boundary element method in acoustics," Katholieke Universiteit Leuven, Belgium, Mechanical Engineering Department, Noise & Vibration research group, Tech. Rep., 2004, In ISAAC 15 - Course on numerical and applied acoustics, Katholieke Universiteit Leuven, Belgium, Mechanical Engineering Department, Noise & Vibration research group, URL: https://www.isma-isaac.be.

[34] J. Wind, Y. Wijnant, and A. de Boer, "Fast evaluation of the Rayleigh integral and applications to inverse acoustics," in *Proceedings of the ICSV13, The Thirteenth International Congress on Sound and Vibration, Vienna, Austria, July 2-6, 2006*. International Institute of Acoustics and Vibration (IIAV), 07 2006, pp. 1–8.

[35] S. Kirkup and A. Thompson, "Computing the acoustic field of a radiating cavity by the boundary element - rayleigh integral method (BERIM)," in *Proceedings of the World Congress on Engineering, WCE 2007, London, UK, 2-4 July, 2007*, ser. Lecture Notes in Engineering and Computer Science, S. I. Ao, L. Gelman, D. W. L. Hukins, A. Hunter, and A. M. Korsunsky, Eds. Newswood Limited, 2007, pp. 1401–1406.

[36] S. Kirkup, "The boundary element method in acoustics: A survey," *Applied Sciences*, vol. 9, no. 8, 2019. [Online]. Available: https://www.mdpi.com/2076-3417/9/8/1642

[37] F. Gérard, M. Tournour, N. Masri, L. Cremers, M. Felice, and A. Selmane, "Acoustic transfer vectors for numerical modeling of engine noise," *Sound and Vibration*, vol. 36, pp. 20–25, 07 2002.

[38] R. Citarella, L. Federico, and A. Cicatiello, "Modal acoustic transfer vector approach in a fem–bem vibro-acoustic analysis," *Engineering Analysis with Boundary Elements*, vol. 31, no. 3, pp. 248–258, 2007. [Online]. Available: https://www.sciencedirect.com/science/article/pii/S0955799706001688

[39] M. S. Allen and M. W. Sracic, "A new method for processing impact excited continuous-scan laser doppler vibrometer measurements," *Mechanical Systems and Signal Processing*, vol. 24, no. 3, pp. 721 – 735, 2010. [Online]. Available: https://doi.org/10.1016/j.ymssp.2009.11.004

[40] D. Di Maio and D. J. Ewins, "Continuous scan, a method for performing modal testing using meaningful measurement parameters; Part I," *Mechanical Systems and Signal Processing*, vol. 25, no. 8, pp. 3027 – 3042, 2011. [Online]. Available: https://doi.org/10.1016/j.ymssp.2011.05.018

[41] J. Baqersad, P. Poozesh, C. Niezrecki, and P. Avitabile, "Photogrammetry and optical methods in structural dynamics - A review," *Mechanical Systems and Signal Processing,* , 2016, Elsevier Science Ltd. [Online]. Available: https://doi.org/10.1016/j.ymssp.2016.02.011

[42] R. Del Sal, L. Dal Bo, E. Turco, A. Fusiello, A. Zanarini, R. Rinaldo, and P. Gardonio, "Vibration measurements with multiple cameras," in *Proceedings of the ISMA2020 including USD2020 - International Conference on Noise and Vibration Engineering, Leuven, Belgium, September 7-9*. KU Leuven, September 7-9 2020, pp. 2275–2292, Optical methods and computer vision for vibration engineering, paper ID 481.

[43] R. Del Sal, L. Dal Bo, E. Turco, A. Fusiello, A. Zanarini, R. Rinaldo, and P. Gardonio, "Structural vibration measurement with multiple synchronous cameras," *Mechanical Systems and Signal Processing*, vol. 157, p. 107742, 2021. [Online]. Available: https://www.sciencedirect.com/science/article/pii/S0888327021001370

Appendix

A Nomenclature

DIC	Digital Image Correlation	NVH	Noise and Vibration Harshness
dof	degree of freedom	ODS	Operative Deflection Shape
EFFMA	Experimental Full Field Modal Analysis	SLDV	Scanning Laser Doppler Vibrometer
EMA	Experimental Modal Analysis	(ω)	frequency dependency
ESPI	Electronic Speckle Pattern Interferometry	$\mathbf{X}(\omega)$	displacement map
FRF	Frequency Response Function	$\mathbf{F}(\omega)$	excitation forces
NDT	Non Destructive Testing	$\mathbf{H_d}(\omega)$	*Receptance* map